International Journal of Science and Research Archive

eISSN: 2582-8185

Cross Ref DOI: 10.30574/ijsra

Journal homepage: https://ijsra.net/

(Research Article)

Assessment of groundwater quality with ordinary kriging, empirical Bayesian kriging and radial basis function spatial interpolation techniques: Case study of Asaba

Jeff Oba *, Robert Ogaga Onosakponome and Joachim Chinonyerem Osuagwu

Department of Civil Engineering, School of Engineering and Engineering Technology, Federal University of Technology, Owerri Nigeria.

International Journal of Science and Research Archive, 2026, 20(01), 694–713

Publication history: Received on 11 June 2026; revised on 17 July 2026; accepted on 20 July 2026

Article DOI: https://doi.org/10.30574/ijsra.2026.20.1.1498

Abstract

Groundwater stands as a primary source of drinking water in Asaba coastal region with significant influence on human health and ecological system. Hence, evaluating its quality is of paramount importance. This study investigates the spatial variability of groundwater quality in Asaba region and aim to predict conditions at unsample locations. To actualize this, physiochemical parameters and some selected heavy metals were analyzed from 62 water sampling locations. The parameters measured include Total Suspended Solids, Temperature, Acidity, as $CaCO_3$, Alkalinity, as $CaCO_3$, Magnesium, Lead (Pb), Nickel (Ni), and Zinc (Zn). This results were then compared against the World Health Organization permissible limits for drinking water. Descriptive statistical measures including Shapiro-Wilk test to confirmed normality satisfying the distributional requirement for Ordinary Kriging without data transformation were applied to evaluate the distribution of groundwater quality parameters. To predict values at unsampled location in the study area, empirical Bayesian kriging (EBK), Ordinary kriging (OK) and Radial basis functions (RBFs) were employed. The experimental variogram parameters were estimated using OK approach resulting in spherical model. Cross-validation statistics were then used to assess the performance of OK technique. Finally spatial distribution maps of groundwater quality were generated using EBK, OK and RBF categorized into five distinct of various classes.

Keywords: Groundwater; Kriging interpolation; Radial basis Functions; Asaba

1. Introduction

Water constituents an indispensable resource for nurturing survival and development of life on the earth. Ground and surface water are important source of water which are indispensable in supporting agriculture industry and human livelihood. However, in Nigeria and other developing nations, the combine effects of climate variability and anthropogenic drivers such as demographic expansion, industrial growth and urbanization has led to significant deterioration in water resource availability and quality (Singh et al., 2016). Nigeria is considered to be abundantly blessed with water resources, surface (267.3BCM), ground (51.9BCM), however these resources are polluted by indiscriminate disposal of waste, lack of proper sewerage system, unregulated cottage industries, automotive repairs shops, oil spillage and open air defecation etc (National water Resource Policy, 2016, Ibrahim et al., 2022).

In Nigeria, an estimated 60% of sewage effluent is released untreated into rivers leading to a decline both in availability of the resource and in quality (UNN 2025), especially in the northern and northeastern regions where aquifer have dropped by 10 -15meters due to the over –abstraction for urban use, industrial demand and for agricultural purposes (Ibrahim et al., 2022). The World bank (2017) reported in its Nigeria Water supply Sanitation and Hygiene Poverty Diagnostic that approximately only 29% of the population have access to safe water source while a larger percentage of the population lack access.

Asaba, functions as a key industrial region that plays a significant role in driving Nigeria economic growth, especially as population drift from Onitsha as a result of sit at home on Mondays halting business, most industries have relocated to Asaba increasing its population and such industries includes pharmaceutical, fertilizer and agro industry, steel, automobile repairs, textile, rice, fuelling stations, discharging their wastes into rivers and groundwater. As a result the problem of water pollution arises by placing detrimental impacts on human and ecological systems (NESREA, 2007). It is therefore vital to examine the spatial distribution of pollutants groundwater so as to design effective management strategies and map pollutant concentrations. Extensive studies by different researchers have demonstrated the use of geographic information system (GIS) and statistical tools for water quality mapping and monitoring. Geostatistics technique estimates values at unsampled places with less sparse sample data when considering space (Oliver and Webster, 1991).

Spatial interpolation techniques are divided into deterministic and geostatistical categories. Deterministic methods uses mathematical functions to estimates values at unsample sites, while geostatistical method incorporate spatial autocorrelation among data points to yield surfaces that reflect inherent spatial dependence thereby enhancing predicative accuracy in unsampled regions (Gunnink & Burrough, 2019). Geospatial methods includes Ordinary Kriging (OK), Simple Kriging (SK), Universal Kriging (UK) and Empirical Bayesian Kriging (EBK) while deterministic method includes Local Polynomial Interpolation (LPI) and radial basis functions. (Bhunia, et al., 2018).

Ayalew and Tegenu (2024) conducted a study examining the spatial distribution and trends of groundwater pollutant in Gurage, Ethiope. The research reveals contamination hotspot linked to natural geochemical processes and anthropogenic influences. A total of twenty seven samples were collected from various sites and analyzed. Chaudhry et al. (2019) examined groundwater contamination in Punjab Rupnagar district, applying an integrated methodology that combined exploratory factor analysis (EFA) and ordinary kriging (OK). Agyemang (2022) conducted application of geostatistical techniques in the assessment of groundwater contamination in the Afgya Kwabre District of Ghana.

The aim of the present study is (i) to assess groundwater quality using three interpolation method namely: Ordinary kriging, Empirical Bayesian kriging and Radial Basis Function, (ii) identify high and low-concentration areas and spatial distribution map to guide for effective remediation efforts to address pollution levels across the study area.

2. Methodology

2.1. Study area and data sampling

The study area is situated within Oshimili North and South, Local Government Areas of Delta State, South-South Region. It spans at latitude 6°8′ N to 6°16′ N and longitudes 6°36′E to 6°45′E (Fig. 1). Asaba is strategic located with river Niger at its boundary on one lane approach, having Oko market mainly occupied by the Hausa people. There is a wood market and motor repairs industries in the ontisha-Asaba express road. It major market is ogbeogonogo market and cable point market that shares boundary with the river Niger where most waste are emptied to.

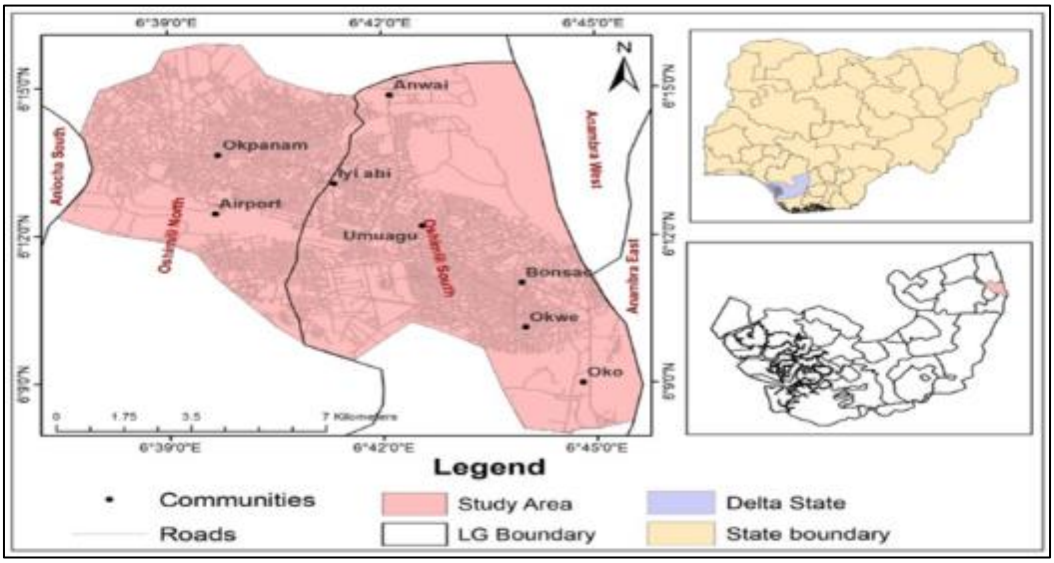

Figure 1 The Locational Map of Asaba

Fieldwork was conducted in October 2025 during which data were collected from 62 boreholes across the study area as in Fig 2. The equipment used includes a GPS device, cameras, timer, plastic bailer, cooler box pen marker, dip meter and transparent 2 liter plastic bottles. For each sampling point, coordinates, well depth along with date and time were systematically recorded.

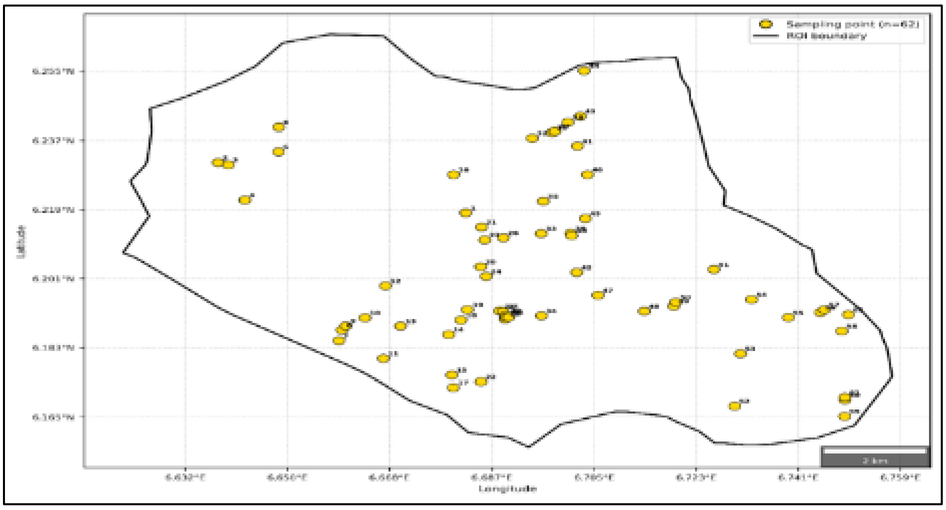

Figure 2 Sampling locational Map

Prior to collecting water samples from the selected boreholes, the borehole was flushed to remove stagnant water in ensuring sample represented actual groundwater. Distilled water was used to rinse each sample bottles then filled with 20 ml of groundwater, sealed and shielded from direct sunlight. All bottles were marked with date and time of collection, then store in the cooler boxes to facilitate transport from field to the laboratory. Recorded field data were transfer into Microsoft excel and imported into a GIS system to create point maps which were subsequently used to generate spatial distribution maps by the three interpolation methods.

2.2. Lab analysis of water samples

Water samples from 62 boreholes were transported to the laboratory within 48 hours of collection for further analysis. Sampling and analytical procedure adhered to the guidelines of the American Public Health Association and WHO standards. The groundwater parameters examined included total Suspended Solids, Temperature, acidity as $CaCO_3$, Alkalinity as $CaCO_3$, Magnesium (Mg), Lead (Pb), Nickel (Ni), and Zinc (Zn). Temperature was measured using the probe method, while concentration of lead, magnesium, zinc and nickel were determined through flame atomic absorption spectrometry. Total suspended solids were analyzed using photometric method 8006 and acidity and alkalinity were assessed through titration techniques. Table 1 provides the recommended limits for drinking water by WHO and Standards Organization of Nigeria/Nigerian Industrial Standard

Table 1 Recommended permissible limits for potable drinking by SON and WHO guidelines

S/N	PHYSIOCHEMICAL PARAMETERS	WHO	SON/NIS
1	T. S. S (mg/l)	30	-
2	Temperature, ^{0}C	-	-
3	Acidity, mg/L as $CaCO_3$	-	-
4.	Alkalinity, mg/L as $CaCO_3$	-	-
5	Magnesium (Mg) (mg/l)	-	20
6	Lead (Pb) (mg/l)	0.01	0.01
7	Nickel (Ni) (mg/l)	0.07	0.02
8	Zinc (Zn) (mg/l)	5	3

2.3. Variogram models

Variogram models were used in estimating the values of semivarogram parameters that are require for spatial prediction. A semivariogram γ(h) as shown in Equ (i) was applied to detect spatial dependence among neighboring sites since assessing spatial correlation before interpolating unsample location

$$\gamma(h) = \frac{1}{2N}\sum_{i=1}^{N(h)}[z(x_i) - z(x_i + h)]^2 \qquad (1)$$

Where;
z (x_i) and z(x_i+ h)=are the studied variable values at locations xi and (xi + h)
h = lag or distance interval
N (h) = is the number of observation pairs separated by a distance h
γ(h)= estimated or experimental semivariance value for all pairs at a lag distance h
〖x〗_i=the georeferenced positions where z (x_i) values were measured

For parameters that did not follow a normal distribution, Box-cox transformation as given in Equ. 2 was employed.

$$Y' = \begin{cases} \frac{Y^{\lambda} - 1}{\lambda} & \lambda \neq 0 \\ \log(Y) & \lambda = 0 \end{cases} \qquad (2)$$

Where Y' is the transformed variable and λ is the transformation parameter.

The Shapiro–Wilk (1965), normality test was applied to evaluate the normality of groundwater quality parameters which is the first stage of interpolation method as presented in Table 2. Model such as sine hole effect, circular, power, spherical, exponential, Gaussian, and among others can be used to fit a semivariogram. Fitted semivariogram is usually characterized by three measures; the nugget, the range and the sill. Nugget effect is the variability seen between samples that are closely spaced. Range is the distance after which the variogram levels off, that is the distance at which the semivariogram reaches the sill and sill is the distance at which the data is no longer correlated. Using h to represent lag distance, c_n to represent nugget effect, α to represent range, σ to represent partial sill and c_o to represent sill which consists of the nugget effect, if present and the partial sill; c_o= c_n+ σ. As shown in the Fig 3. (Bohling, 2005; Chang, 2014).

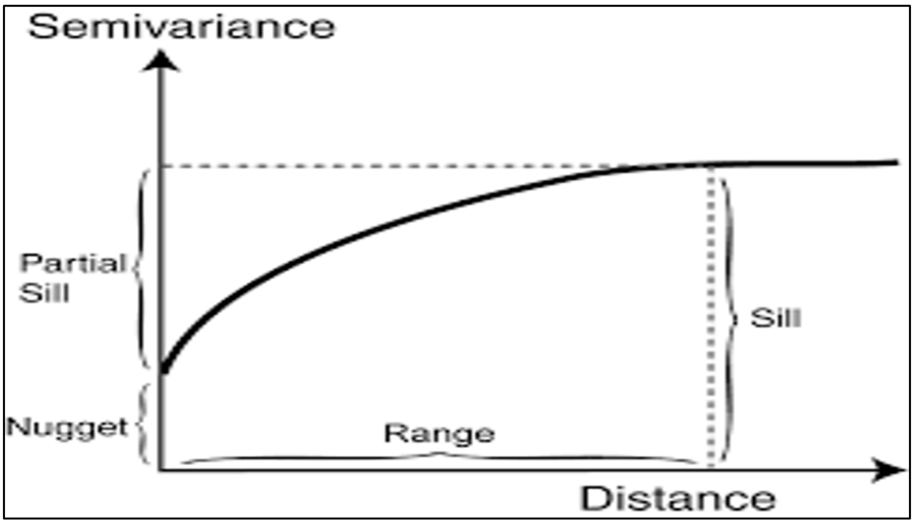

Figure 3 Semivariogram with range, sill and nugget effect (ESRI, 2010)

Some of the models are shown in Equ 3 to 8 (Bohling, 2005) below;

$$Spherical\ (h) = \begin{cases} 0 & if\ h = 0 \\ c_n + \sigma\left(1.5\left(\frac{h}{a}\right) - 0.5\frac{h^3}{a}\right) & if\ h \le a \\ c_o & if\ a < h \end{cases} \quad (3)$$

$$\text{Circular } \gamma\ (\text{h}) = \begin{cases} \text{c}_\text{n} + \sigma\left(1 - \frac{2}{\pi}\cos^{-1}\left(\frac{\text{h}}{\text{a}}\right) + \sqrt{1 - \frac{\text{h}^2}{\text{a}^2}}\right) & \text{if h} \le \text{a} \\ \text{c}_\text{o} & \text{if h} > a \end{cases} \quad (4)$$

$$Exponential{:} \quad y\ (h) = c_n + \sigma\left(1 - \exp\left(\frac{-h}{a^2}\right)\right) \quad (5)$$

$$Guassian{:} \quad y\ (h) = c_n + \sigma\left(1 - \exp\left(\frac{-h^2}{a^2}\right)\right) \quad (6)$$

$$\text{Power; } \gamma\ (\text{h}) = \text{c}_\text{n} + \sigma\text{h}^\text{a} \quad \text{with } 0 < a < 2 \quad (7)$$

$$\text{Sine hole effect; } \gamma\ (\text{h}) = \text{c}_\text{n} + \sigma\left(1 - \frac{\sin\left({}^{\pi\text{h}}/_{\text{a}}\right)}{{}^{\pi\text{h}}/_{\text{a}}}\right) \quad (8)$$

2.4. Spatial interpolation techniques

(i.).Ordinary Kriging (OK) is a generally accepted method which is applied for interpolation geostatistically. The weights in Ordinary kriging are determined through the kriging equation given in Equ 9 that are derived from the function of the semivariogram (Xie, 2011).

$$Z(x_0) = \sum_{i=1}^{n} \lambda i . Z(x_i)\ with \sum_{i=1}^{n} \lambda i = 1 \quad (9)$$

Where Z(x0) is the random variable at the location x0, Z(xi) is the measured value at a location xi, λi is the weighting factor assigned to Z(xi) and n is the number of observations (Bradaï et al., 2016).

Ordinary kriging is regarded as a linear unbiased estimator as it estimates are calculated through a weighted linear summation of the present data, and unbiased because it seek to have a mean error of zero. It purpose is to minimize the variance of the estimation errors which keeps OK from other techniques.

ii). Empirical Bayesian Kriging (EBK) is an automated interpolation techniques that separates itself from other kriging methods by optimizing the parameters of the spatial process and incorporating estimation errors into the semivariogram model. Also EBK engages intrinsic random functions as it kriging framework to enhance the robustness and accuracy of the spatial prediction (Samsonova et al., 2017; ESRI, 2019).

(iii) Radial basis functions (RBF's) are set of exact interpolator that are design to generate smooth surfaces from available large dataset that require the surface to pass through all measured points (ESRI, 2019). The fundamental equation of RBF rely on the distance between predicted and observed values (Xie, et al., 2011). The interpolation equation Z(x), is given as the sum of two component as shown in Equ 10 and a trend function T(x) as given in Equ. 11

$$Z(x) = T(x) + \sum_{j=n}^{N} \lambda_j \ R(d_j) \quad (10)$$

$$T(x) = \sum_{i}^{M} a_i \ f_i\ (x) \quad (11)$$

Where fi(x) is a set linearly independent functions, R (dj) is a radial basis function and dj is the distance between the measured and the predicted location. Once R(dj) is known, coefficients ai and λi can be calculated.

2.5. Cross-validation

The effectiveness of the interpolation techniques was assessed using cross validation statistics and the commonly used measures include Ok, EBK and RBFs evaluated alongside mean error (ME) and root mean square error (RMSE). These statistics can be calculated using mathematical Equ 12 and 13 (Fallah et al, 2019). The model that yields the lowest ME and RMSE values is regarded as the most accurate.

$$ME = \frac{1}{n}\sum_{i=1}^{n}[Z(X_i) - Z^i(X_i)] \qquad (12)$$

$$RMSE = \sqrt{\frac{1}{n}\sum_{i=1}^{n}[Z(X_i) - Z^i(X_i)]^2} \qquad (13)$$

Where Z' (xi) is the estimated measure of the same location

3. Results and discussion

3.1. Descriptive analysis

Table 2 presents the descriptive analysis of the physiochemical groundwater quality parameters that includes: Total Suspended Solids, Temperature, Acidity as $CaCO_3$, Alkalinity as $CaCO_3$, Magnesium (Mg), Lead (Pb), Nickel (Ni), and Zinc (Zn) measured from 62 borehole sites across Asaba. Descriptive and geostatistical analyses were performed using Microsoft Excel and ArcGIS 10.7. The Shapiro–Wilk normality test (Table 2) confirmed that the water quality parameters follow a normal distribution. Semivariograms were fitted independently for all 8 parameters. Three candidate models were tested for each parameter (Spherical, Exponential, Gaussian), and the best fit was selected by lowest RMSE from leave-one-out cross-validation. Fitting was carried out in Python using pykrige with automatic optimization, without forced initial parameters. Fitted values for all parameters are shown in Table 3. The Nugget-to-Sill Ratio (NSR) classification follows Cambardella et al. (1994): < 0.25 = Strong, 0.25 to 0.75 = Moderate, > 0.75 = Weak spatial dependence

Table 2 Statistical analysis of groundwater quality parameters

Parameter	N	Mean	Median	Minimum	Maximum	Variance	Std Dev	CV (%)	Skewness	Kurtosis	K-S test (p)
Total Suspended Solids (mg/L)	62	0.0482	0.0000	0.0000	0.9200	0.0267	0.1633	338.66	4.0533	16.8144	0.0000
Temperature (°C)	62	28.8710	29.0000	25.0000	30.0000	1.3352	1.1555	4.00	-1.2402	1.2241	0.0000
Acidity (mg/L as CaCO3)	62	26.7277	24.7500	6.9000	58.0000	222.5526	14.9182	55.82	0.2857	-1.1565	0.0909
Alkalinity (mg/L as CaCO3)	62	14.8565	9.0000	2.0000	30.0000	100.4523	10.0226	67.46	0.3612	-1.5868	0.0009
Magnesium (mg/L)	62	2.1523	1.6350	0.1900	6.1000	2.6286	1.6213	75.33	1.2374	0.2619	0.0150
Lead (mg/L)	62	0.0004	0.0000	0.0000	0.0010	0.0000	0.0005	131.28	0.5342	-1.7146	0.0000
Nickel (mg/L)	62	0.0003	0.0000	0.0000	0.0010	0.0000	0.0005	151.67	0.8397	-1.2950	0.0000
Zinc (mg/L)	62	0.0741	0.0795	0.0000	0.1800	0.0010	0.0311	41.96	-0.0706	1.3944	0.3066

Table 3 Fitted semivariogram parameters for all 10 parameters

Parameter	Model	Nugget	Partial Sill	Total Sill	Range (m)	NSR	Dependence
TSS	Spherical	0.000	0.069	0.069	13,677	0.000	Strong
Temperature	Spherical	0.185	1.111	1.296	1,284	0.143	Strong
Acidity	Spherical	64.334	203.5	267.9	6,815	0.240	Strong
Alkalinity	Spherical	38.549	75.757	114.306	2,515	0.337	Moderate
Magnesium	Spherical	1.361	2.948	4.309	7,159	0.316	Moderate
Lead	Exponential	0.000	0.000	0.000	3,419	—	—
Nickel	Gaussian	0.000	0.000	0.000	3,419	0.690	Moderate
Zinc	Spherical	0.000	0.001	0.001	1,030	0.089	Strong

Fig 4(a) and 4(b) display the semivariogram models for total suspended solids (TSS) and temperature. The best fit models are acceptable having mean square error (MSE) values close to zero. As shown in Table 4, there is strong consistency between root mean square error (RMSE) and mean absolute error (MAE) for both pollutants. The RMSE of the best fit model for TSS is 0.20 while for temperature is 1.2951. The semivariogram model for TSS follows a spherical structure with a nugget-to –sill ratio of 0% indicating very strong spatial correlation. In comparison, the temperature model has a nugget-to-sill ratio of 14.3% also reflecting strong spatial correlation. These outcomes are in line with the findings of Ayalew and Tegenu (2024), who likewise applied spherical model in their study.

Table 4 Cross validation of ordinary kriging

Parameters	ME	RSME	MAE
TSS	-0.0023	0.2000	0.0799
Temperature	+0.0074	1.2951	0.9502
Acidity	-0.0759	10.9658	7.3347
Alkalinity	-0.0437	7.3819	5.8755
Magnesium	-0.0186	1.0748	0.7954
Lead	0.0000	0.0006	0.0005
Nickel	-0.0027	0.2473	0.1168
Zinc	+0.0005	0.0319	0.0227

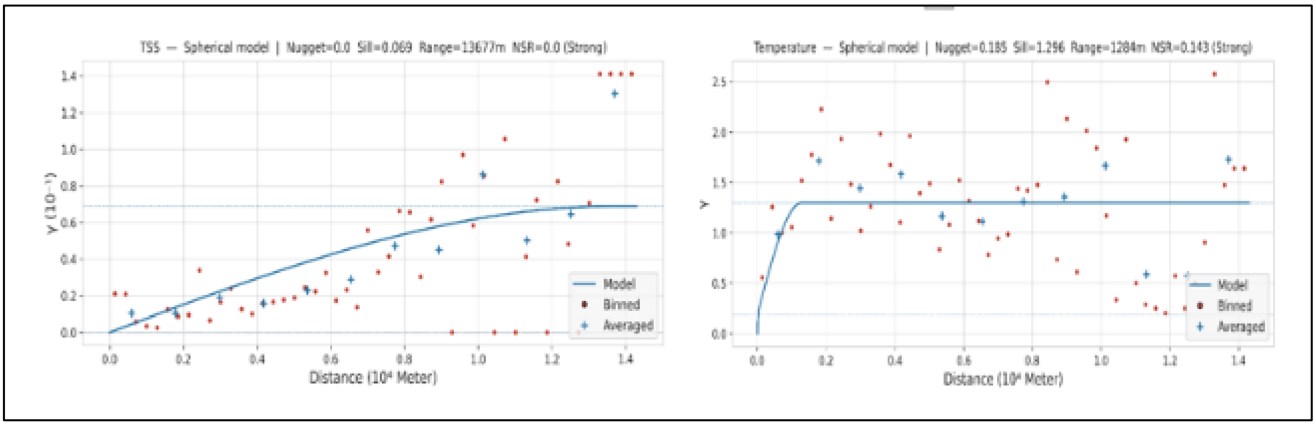

Figure 4 (a) semivariogram model of TSS concentration (b) Semivariogram model for Temperature

Figure 5(a) and 5(b) shows the semivariogram model for Acidity and Alkalinity. The best-fit semivariogram models are deemed reliable with ME values approaching zero. As shown in Table 4, there is clear consistency between RMSE and MAE for the pollutants

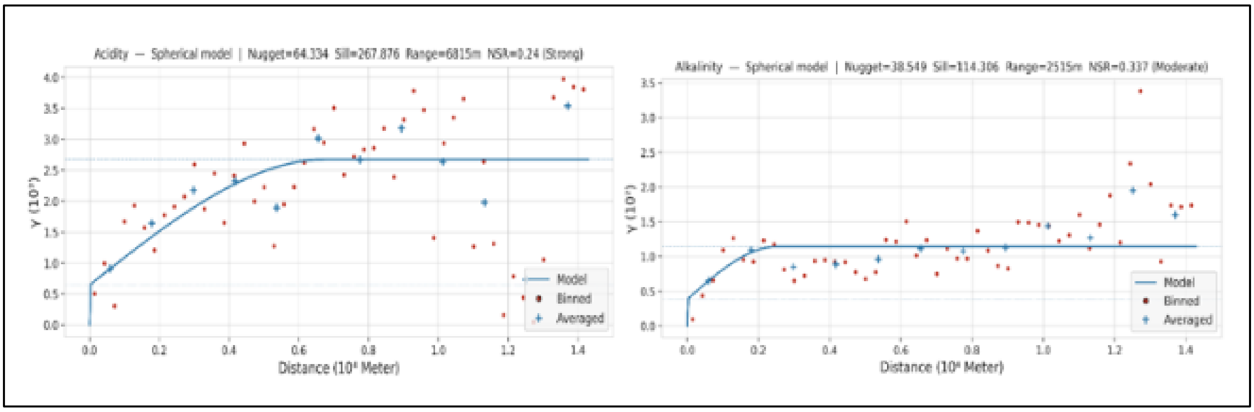

Figure 5 (a) Semivariogram model for Acidity (b) semivariogram model for Alkalinity concentration

The semivariogram models used for Acidity is spherical with nugget-to-sill ratio of 24% indicating strong spatial correlation while for alkalinity nugget to sill ratio is 33.7% reflecting moderate spatial correlation. Fig 6(a) and 6(b) shows the semivariogram model for magnesium and lead. The best-fit semivariogram models are deemed reliable with ME values approaching zero. As shown in Table 4, there is clear consistency between RMSE and MAE for the pollutants.

RMSE values of the best-fitted models for magnesium is 1.0748 while for lead is 0.0006. The semivariogram models used for magnesium is spherical with nugget to sill ratio is 46.2% indicating moderate spatial correlation while for lead nugget to sill ratio is 69.3% reflecting moderate spatial correlation

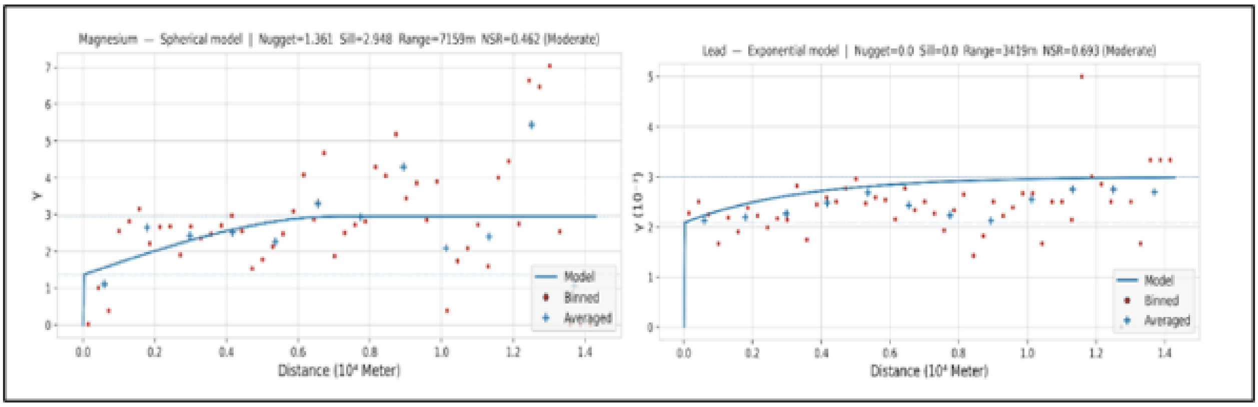

Figure 6 Semivariogram model (a) for Magnesium (b) lead concentration

Fig 7(a) and 7(b) shows the semivariogram model for nickel and zinc. The best-fit semivariogram models appear acceptable, with MSE values close to zero. As shown in Table 4, there is clear consistency between RMSE and MAE for the pollutants. RMSE values of the best-fitted models for nickel is 0.2473 while for zinc is 0.0319.

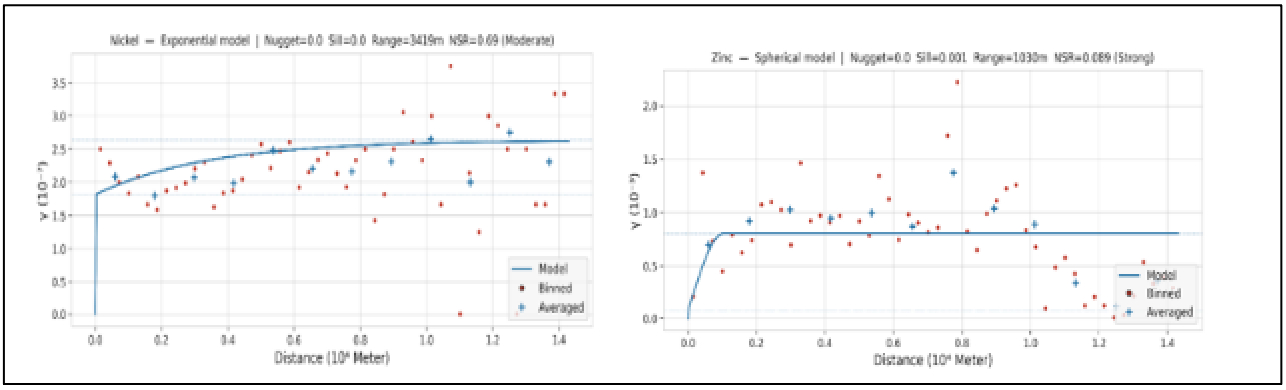

Figure 7 Semivariogram model for (a) Nickel (b) Zinc concentration

The semivariogram models used for nickel is spherical however it nugget to sill ratio is 69% indicating moderate spatial correlation while for zinc nugget to sill ratio is 8.9% indicating strong spatial correlation

Three interpolation methods were applied to all eight parameters. All outputs were generated at 30-metre resolution, clipped to the study area ROI polygon boundary, and saved as GeoTIFF files. Prediction maps were classified using Natural Breaks (Jenks) into five classes.

Ordinary Kriging (OK): where each parameter was interpolated using its own fitted semivariogram (model, nugget, partial sill, and range from Table 3). Empirical Bayesian Kriging (EBK) is Power semivariogram model, auto-fitted internally and its settings is 50 maximum local points with overlap factor 1, 100 simulated semivariograms, and prediction output type. Radial Basis Function (RBF) is Multiquadric kernel function and No semivariogram required.

3.2. Total Suspended Solids

Fig 8(a) OK, 8(b) EBK 8(c)RBF depicts the spatial distribution of TSS in Asaba. The groundwater quality ranged (≤ 0.15, ≤ 0.06, ≤ 0.16) is the dominant class for OK, EBK, and RBF, respectively, and are situated in the northern, eastern, central and west of Asaba. Table 5 shows the surface areas of different TSS categories estimated using EBK, OK and RBF which classes are below WHO limit. The comparison of the three predicted maps generated using RBF, EBK and OK reveals that they share similar overall structure despite difference in used categories and the theoretical basis of each method. This consistency validates the results obtained for the spatial distribution of spatial TSS concentration in Asaba region.

Table 5 Surface areas of different TSS categories estimated using EBK, OK and RBF

OK — Categories	**Area (km^2)**	**Area (%)**	**EBK — Categories**	**Area (km^2)**	**Area (%)**	**RBF — Categories**	**Area (km^2)**	**Area (%)**
≤ 0.15	101.921	86.51	≤ 0.06	78.526	66.65	≤ 0.16	102.343	86.86
0.15 – 0.34	8.500	7.21	0.06 – 0.12	24.086	20.44	0.16 – 0.34	8.105	6.88
0.34 – 0.52	4.285	3.64	0.12 – 0.18	7.048	5.98	0.34 – 0.53	4.441	3.77
0.52 – 0.71	2.876	2.44	0.18 – 0.24	5.117	4.34	0.53 – 0.71	2.696	2.29
> 0.71	0.238	0.20	> 0.24	3.045	2.58	> 0.71	0.236	0.20
Total	117.820	100.00	Total	117.822	100.00	Total	117.821	100.00

Findings in Fig 8 (a) show that the concentrations of the values ranges from (≤ 0.15, colour coded dark blue Okpanam, Isele-Asagba, Ogbe-ozoma, Umuonaje, Isieke, Cable point, Ezenei, Airpot, indicating cleaner peripheral waters likely influenced by reduced anthropogenic activity or natural sedimentation. (0.15 – 0.34) with Lavender color coded is found in Anwai area, reflecting urban runoff and riverine transport (0.34 – 0.52) with white colour is found in southern area, (0.52 – 0.71) with Mauve colour coded is found also in southern area of oko, and (>0.71) is found in head bridge mark hotspots of severe sediment accumulation from erosion, industrial discharge, or construction.

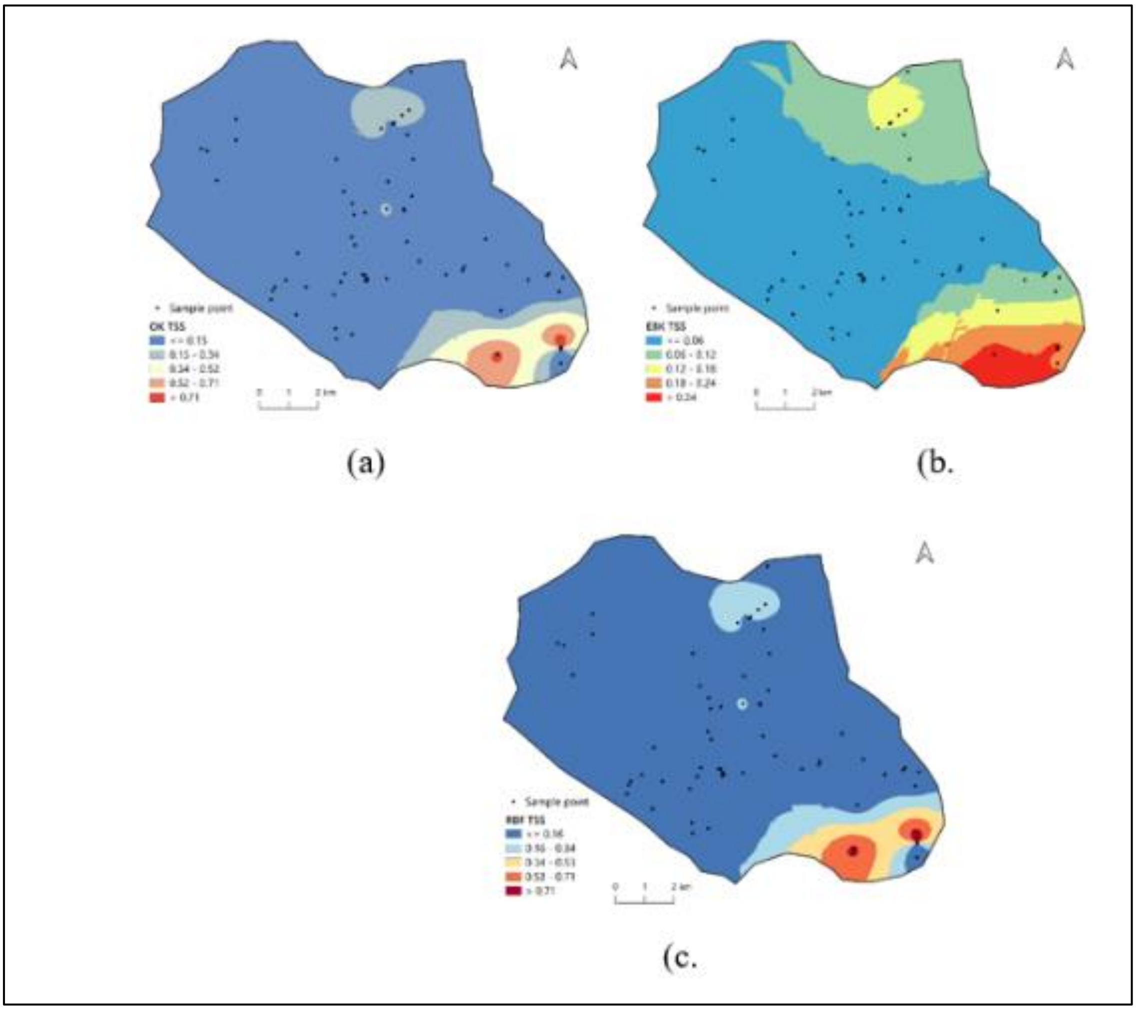

Figure 8 Spatial distribution of TSS across Asaba (a) OK, (b). EBK (c) RBF

3.3. Temperature

Fig 9 (a) OK, 9(b) EBK and 9(c) RBF shows a clear spatial gradient in near-surface temperature across Asaba, Delta State and Table 6 shows the surface areas of different temperature categories estimated using EBK, OK and RBF. The findings in this Figures shows intermediates values concentrated in the eastern, western and south-eastern zones and higher values in the northern and southern sectors. For instance, temperatures range around the Airport–Okpanam–Iyi Abi–Umuagu axis is dominated by temperature class of 28.05 – 29.02◦C (rust tones), forming a contiguous warm core likely reflects dense built-up land, higher anthropogenic heat, and reduced vegetation cover. In contrast, peripheral communities such as Bonsac, Okwe and Oko fall largely within the upper temperature classes of >29.02 ◦C (dark brown), indicating relatively cooler micro climates that are consistent with lower building density and higher vegetation or open space

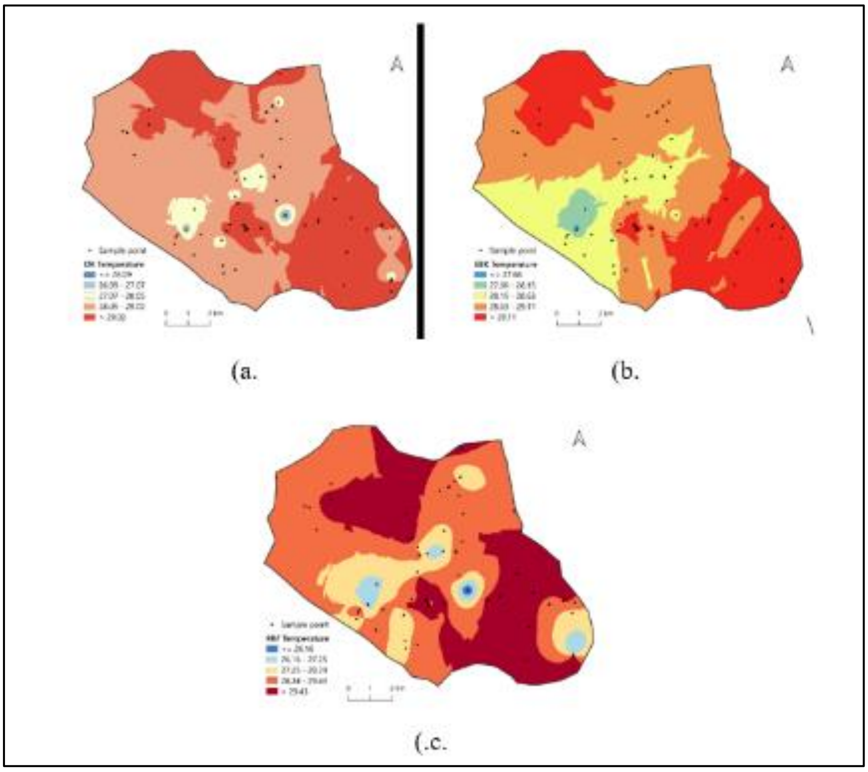

Figure 9 Spatial distribution of Temperature across Asaba (a) OK, (b). EBK (c) RBF

Table 6 Surface areas of different Temperature categories estimated using EBK, OK and RBF

OK — Categories	Area (km²)	Area (%)	EBK — Categories	Area (km²)	Area (%)	RBF — Categories	Area (km²)	Area (%)
≤ 26.09	0.043	0.04	≤ 27.66	0.075	0.06	≤ 26.16	0.157	0.13
26.09 – 27.07	0.318	0.27	27.66 – 28.15	2.840	2.41	26.16 – 27.25	3.054	2.59
27.07 – 28.05	4.983	4.23	28.15 – 28.63	24.542	20.83	27.25 – 28.34	17.721	15.04
28.05 – 29.02	68.565	58.19	28.63 – 29.11	52.828	44.84	28.34 – 29.43	57.317	48.65
> 29.02	43.912	37.27	> 29.11	37.536	31.86	> 29.43	39.572	33.59
Total	117.821	100.00	Total	117.821	100.00	Total	117.821	100.00

This pattern suggests an emerging urban heat island centred on the more urbanized parts of Asaba, with temperatures gradually decreasing towards the less developed fringes. The concentric transition from rust in the core, to dark brown at the edges depicts a systematic spatial distribution that aligns with typical urban–rural thermal contrasts reported in tropical cities. For instance, Adeaga et al. (2019) who documented similar land-surface temperature gradients in Lagos, Nigeria, where dense urban fabrics exhibited significantly higher temperatures than vegetated peri-urban zones. By analogy, the findings in Fig 9 indicate that land-use intensity and surface cover are key controls on the observed temperature fields, with implications for heat-stress risk, energy demand, and the siting of future green infrastructure.

3.4. Acidity

Fig 10(a) OK, 10(b) EBK and 10(c) RBF reveals the spatial distribution of acidity in Asaba. The groundwater with highest acidity quality values is (41.71 < Acidity ≥ 58.0) represent minor class for EBK, OK and RBF, respectively, which are located in the north and the east and transition to lower acidity eastward and southward of the study area. Table 7 shows the surface areas of different acidity categories estimated using EBK, OK and RBF.

Table 7 Surface areas of different Acidity categories estimated using EBK, OK and RBF

OK — Categories	Area (km²)	Area (%)	EBK — Categories	Area (km²)	Area (%)	RBF — Categories	Area (km²)	Area (%)
≤ 26.09	0.043	0.04	≤ 27.66	0.075	0.06	≤ 26.16	0.157	0.13
26.09 – 27.07	0.318	0.27	27.66 – 28.15	2.840	2.41	26.16 – 27.25	3.054	2.59
27.07 – 28.05	4.983	4.23	28.15 – 28.63	24.542	20.83	27.25 – 28.34	17.721	15.04
28.05 – 29.02	68.565	58.19	28.63 – 29.11	52.828	44.84	28.34 – 29.43	57.317	48.65
> 29.02	43.912	37.27	> 29.11	37.536	31.86	> 29.43	39.572	33.59
Total	117.821	100.00	Total	117.821	100.00	Total	117.821	100.00

This urban-core acidity peak suggests influences from atmospheric deposition, industrial effluents, or organic decomposition in densely populated areas, potentially elevating corrosion risks and ecological stress in water systems. The distribution echoes patterns observed by Longe (2017) in Desalination and Water Treatment, who analyzed surface and groundwater pH in Delta State river basins, noting elevated acidity (pH up to 9.8) near Asaba's urban stretches due to pollution loading.

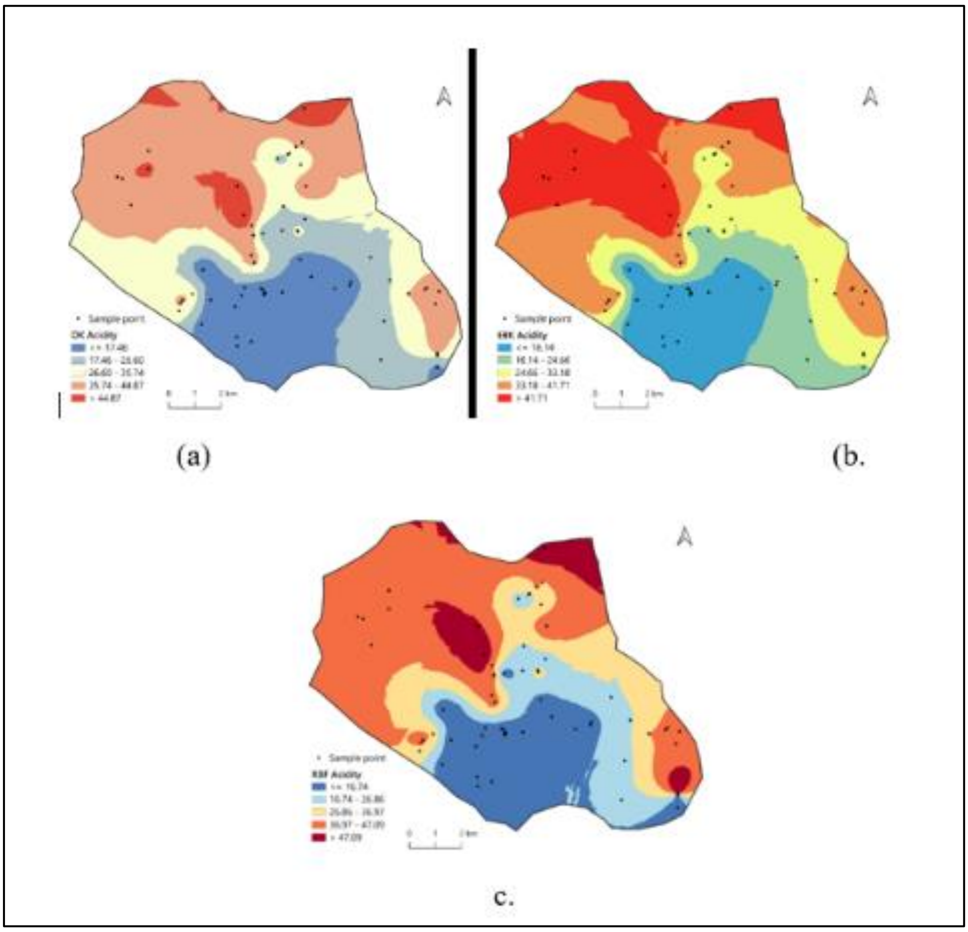

Figure 10 Spatial distribution of Acidity across Asaba (a) OK, (b). EBK (c) RBF

3.5. Alkalinity

Fig 11 (a) OK, 11(b) EBK and 11(c) RBF reveals the spatial distribution of alkalinity in Asaba. The groundwater with highest alkalinity quality values is (21.39 < alkalinity > 26.03) represent minor class for EBK, OK and RBF, respectively, which are located in the east and west of the study area. Table 8 shows the surface areas of different alkalinity categories estimated using EBK, OK and RBF.

Table 8 Surface areas of different Alkalinity categories estimated using EBK, OK and RBF

OK — Categories	Area (km^2)	Area (%)	EBK — Categories	Area (km^2)	Area (%)	RBF — Categories	Area (km^2)	Area (%)
≤ 9.36	31.862	27.04	≤ 8.18	31.099	26.39	≤ 6.85	28.363	24.07
9.36 – 13.37	16.930	14.37	8.18 – 13.83	25.340	21.51	6.85 – 13.24	31.982	27.14
13.37 – 17.38	36.476	30.96	13.83 – 19.48	29.244	24.82	13.24 – 19.64	24.277	20.61
17.38 – 21.39	25.413	21.57	19.48 – 25.13	24.831	21.08	19.64 – 26.03	25.523	21.66
> 21.39	7.140	6.06	> 25.13	7.307	6.20	> 26.03	7.676	6.52
Total	**117.821**	**100.00**	**Total**	**117.821**	**100.00**	**Total**	**117.821**	**100.00**

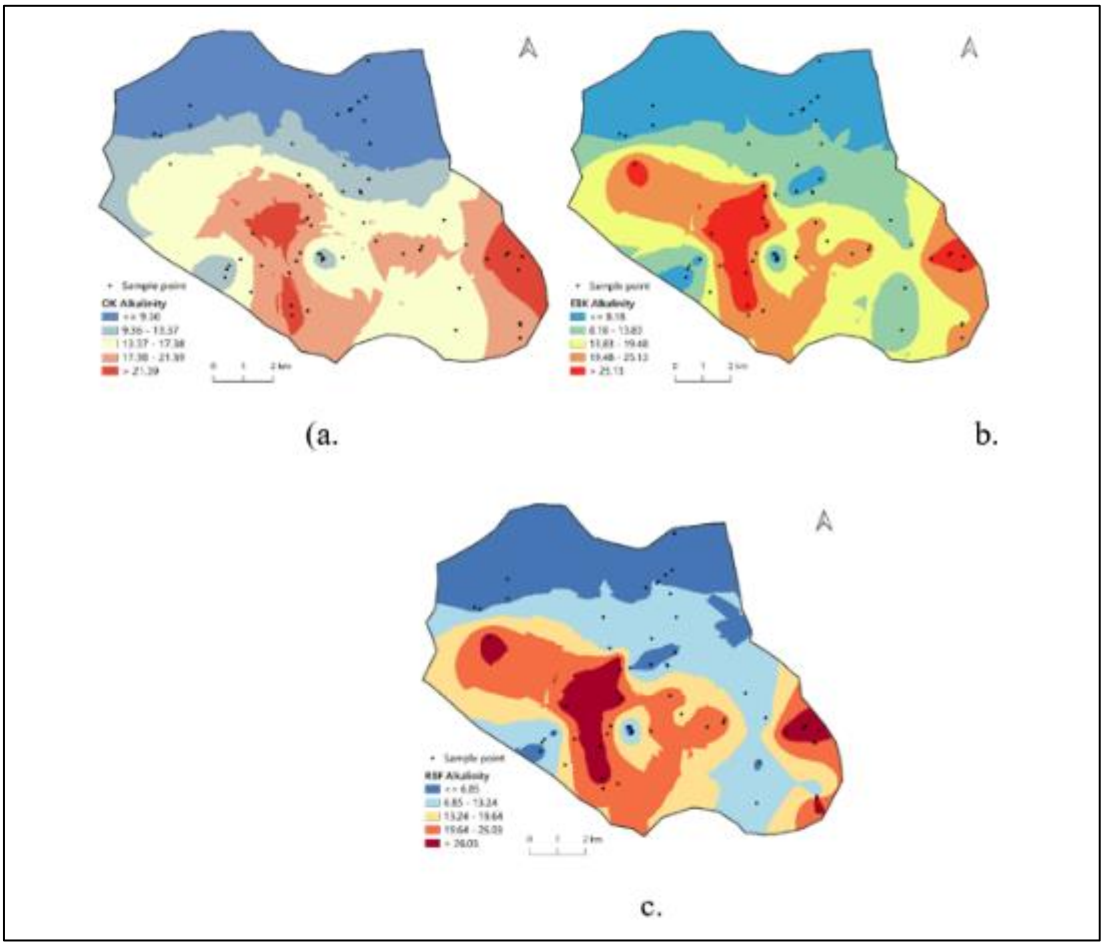

Figure 11 Spatial distribution of Alkalinity across Asaba (a) OK, (b). EBK (c) RBF

The comparison of the three predicted maps using EBK, OK and RBF shows that they have the same general structure despite of the difference in area occupied. In contrast the EBK overestimated the area of this class. This conditions suggest localized geochemical influence from lithology and anthropogenic activities. High alkalinity found around Airport, and Bonsaac indicate high bicarbonate and carbonate concentrations and are likely to experiences intense water-rock interaction. Moderate alkalinity zones found around okpanam and Umuonaje reveals transitional geochemical conditions by mixed lithology and groundwater recharge.

Low alkalinity at Anwai reveals zones where dilution by surface water reduce alkalinity. This study aligns with Nwankwala and Udom 2015 study in Port Harcourt that urbanization increases alkalinity through sewage infiltration and this suggest similar trend in Asaba. However Edet et al, 2011 in contrast reveals that groundwater dominated by calcium bicarbonate type low alkalinity due to silicate weathering while present study shows sodium bicarbonate dominance and higher alkalinity implying stronger carbonate influence. This might be due to the geology of the study areas. Ayalew and Tegenu 2024 in their study done in Ethiope reveals alkalinity ranges of 144.4mg/L - 324.5 mg/L as a result of variations in geological composition

3.6. Magnesium

The following Map, OK Fig 12a), EBK Fig 12b) and RBF, Fig 12c) shows the spatial distribution maps of Magnesium (Mg) concentration indicating the same overall spatial distribution of groundwater magnesium concentration in the study area however the only difference is in the shape and the size of the area of different categories as show in Table 9. The dominants concentration for OK (1.37 -2.54) dark blue color coded is found in north south and east, for EBK (1.38 -2.53) cyan color coded is found in north, central and south and for RBF (1.37 – 2.54) sky blue colour coded is located at north, east and south of the study area which is below the WHO limit.

Table 9 Surface areas of different Magnesium categories estimated using EBK, OK and RBF

OK — Categories	**Area (km^2)**	**Area (%)**	**EBK — Categories**	**Area (km^2)**	**Area (%)**	**RBF — Categories**	**Area (km^2)**	**Area (%)**
≤ 1.37	16.826	14.28	≤ 1.38	19.347	16.42	≤ 1.37	20.798	17.65
1.37 – 2.54	67.258	57.08	1.38 – 2.53	62.965	53.44	1.37 – 2.54	61.910	52.55
2.54 – 3.71	26.055	22.11	2.53 – 3.69	23.779	20.18	2.54 – 3.71	22.501	19.10
3.71 – 4.88	5.573	4.73	3.69 – 4.84	8.771	7.44	3.71 – 4.88	9.375	7.96
> 4.88	2.109	1.79	> 4.84	2.958	2.51	> 4.88	3.236	2.75
Total	**117.821**	**100.00**	**Total**	**117.820**	**100.00**	**Total**	**117.820**	**100.00**

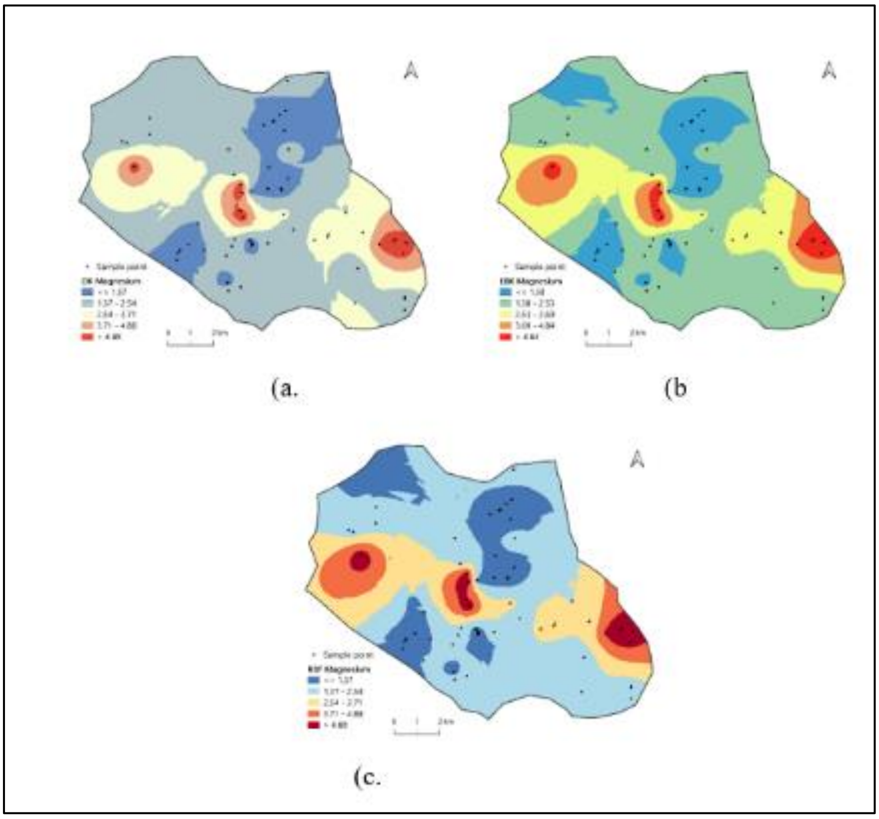

Figure 12 Spatial distribution of Magnesium (Mg) across Asaba (a) OK, (b). EBK (c) RBF

The highest concentration for the three model ranges from ≤ 16.81 > 20.25 with red color code are found in okwe and smallest part of Okpanam. This finding aligns with Agyemang 2022 who have similar magnesium concentration in Ghana with concentration values of 0.02 -17.75mg/L. This might be due to the shared similar geological setting dominated by basement complex rocks and carbonate rich sediments which release magnesium through weathering from dolomite, calcite and Ferro magnesium.

3.7. Lead

The obtained prediction maps for lead is shown in Fig 13 OK (Fig 13a), EBK (Fig 13b) and RBF (Fig 13 c) show the same overall spatial distribution of groundwater Lead-Pb concentration in the study area. The only difference is in the shape and the size of the area of different categories as shown in Table 10. Findings from Fig 13(a) OK reveals that the dominant concentration of lead (≤ 0.06-0.07) light blue colour coded is found in north, east, south and west of the study area however concentration > 0.33 are found ibusa-Asaba area. Fig 13(b) EKB reveals the ranges 0.00032 – 0.00042) yellow colour coded is the dominant class located in north, and central region while Fig 13(c) RBF reveals the ranges ≤ 0.00011) dark blue colour coded as the dominant class located central part of the study area.

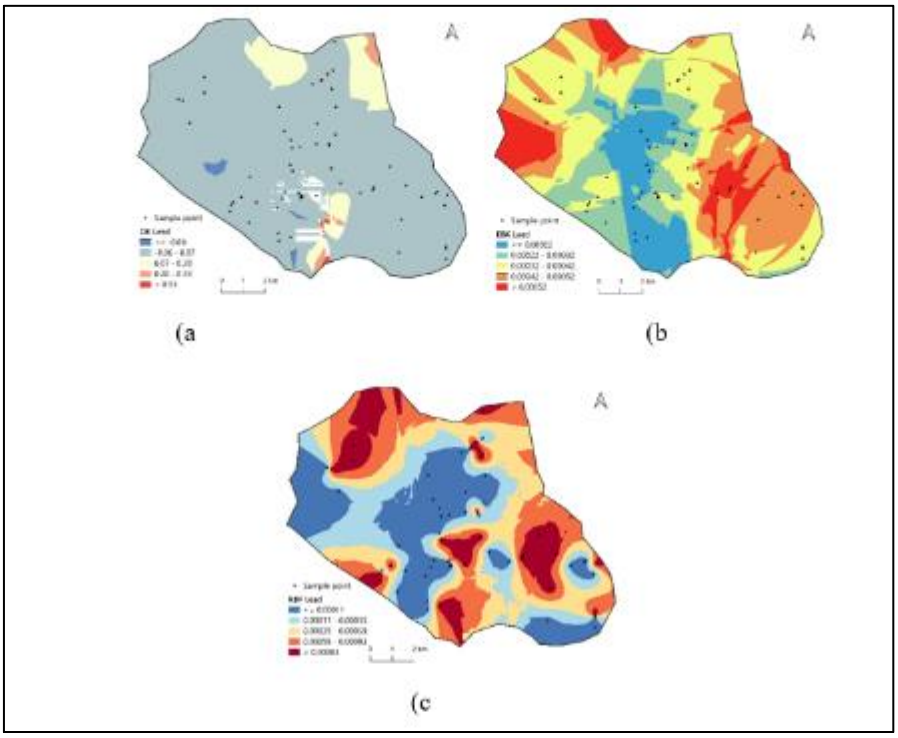

Figure 13 Spatial distribution of Lead across Asaba. (a) OK, (b). EBK (c) RBF

Table 10 Surface areas of different lead categories estimated using EBK, OK and RBF

OK — Categories	Area (km²)	Area (%)	EBK — Categories	Area (km²)	Area (%)	RBF — Categories	Area (km²)	Area (%)
≤ −0.06	0.987	0.84	≤ 0.00022	16.594	14.08	≤ 0.00011	30.238	25.66
−0.06 – 0.07	105.207	89.29	0.00022 – 0.00032	20.124	17.08	0.00011 – 0.00035	22.979	19.50
0.07 – 0.20	10.327	8.76	0.00032 – 0.00042	39.200	33.27	0.00035 – 0.00059	26.814	22.76
0.20 – 0.33	1.127	0.96	0.00042 – 0.00052	29.159	24.75	0.00059 – 0.00083	23.668	20.09
> 0.33	0.173	0.15	> 0.00052	12.743	10.82	> 0.00083	14.122	11.99
Total	**117.821**	**100.00**	**Total**	**117.820**	**100.00**	**Total**	**117.821**	**100.00**

3.8. Nickel (Ni)

The obtained prediction maps for Nickel (Ni) is shown in Fig 14. OK (Fig 14a), EBK (Fig 14b) and RBF (Fig 14c) show the same overall spatial distribution of groundwater nickel concentration in the study area. The only difference is in the shape and the size of the area of different categories as shown in Table 11. Findings from Fig 14(a) OK reveals that the dominant concentration of nickel −0.06 – 0.07) sky blue colour coded is found in north, east ,south and west of the study area however concentration > 0.33 are found Federal Road Safety Corp area Fig 14(b) EKB reveals the ranges 0.00034 – 0.00043 light brown colour coded is the dominant class located in east region while Fig 14(c) RBF reveals the ranges 0.00006 – 0.00032) light blue colour coded as the dominant class covering 33.095km2 (28.09%) of the study area. However other categories are increasing gradually in the study area

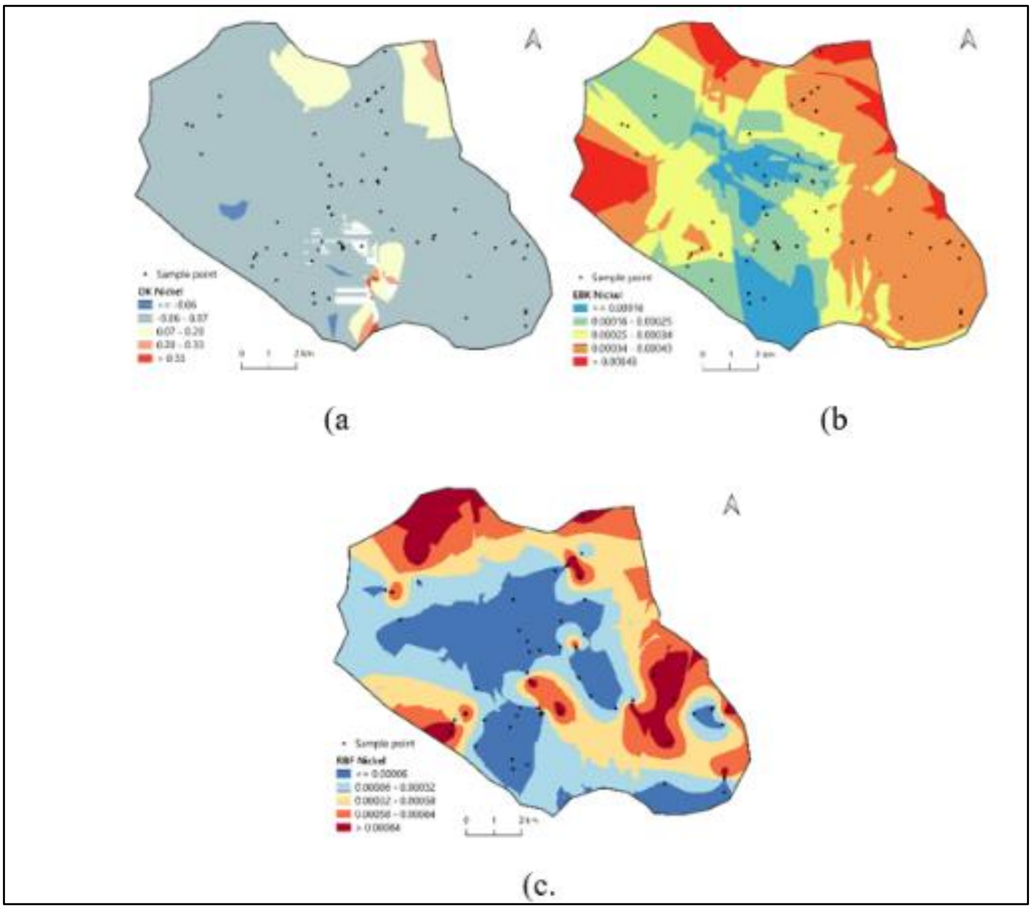

Figure 14 Spatial distribution of Nickel across Asaba. (a) OK, (b). EBK (c) RBF

Table 11 Surface areas of different nickel categories estimated using EBK, OK and RBF

OK — Categories	Area (km^2)	Area (%)	EBK — Categories	Area (km^2)	Area (%)	RBF — Categories	Area (km^2)	Area (%)
≤ −0.06	0.999	0.85	≤ 0.00016	11.984	10.17	≤ 0.00006	30.187	25.62
−0.06 – 0.07	105.208	89.30	0.00016 – 0.00025	23.786	20.19	0.00006 – 0.00032	33.095	28.09
0.07 – 0.20	10.326	8.76	0.00025 – 0.00034	31.515	26.75	0.00032 – 0.00058	26.059	22.12
0.20 – 0.33	1.115	0.95	0.00034 – 0.00043	40.733	34.57	0.00058 – 0.00084	18.928	16.06
> 0.33	0.173	0.15	> 0.00043	9.802	8.32	> 0.00084	9.552	8.11
Total	**117.821**	**100.00**	**Total**	**117.820**	**100.00**	**Total**	**117.821**	**100.00**

3.9. Zinc

The obtained prediction maps is shown in Fig 15. OK (Fig 15a), EBK (Fig 15b) and RBF (Fig 15c) show the same overall spatial distribution of groundwater zinc-Zn concentration in the study area and Table 12 shows the surface areas of the five categories of Zinc estimated using the three interpolation techniques.

Table 12 Surface areas of different Zinc categories estimated using EBK, OK and RBF

OK — Categories	Area (km^2)	Area (%)	EBK — Categories	Area (km^2)	Area (%)	RBF — Categories	Area (km^2)	Area (%)
≤ 0.04	5.281	4.48	≤ 0.04	4.721	4.01	≤ 0.03	4.393	3.73
0.04 – 0.07	23.540	19.98	0.04 – 0.05	4.782	4.06	0.03 – 0.07	33.344	28.30
0.07 – 0.10	88.700	75.28	0.05 – 0.07	12.839	10.90	0.07 – 0.10	76.371	64.82
0.10 – 0.13	0.266	0.23	0.07 – 0.08	53.652	45.54	0.10 – 0.14	3.664	3.11
> 0.13	0.034	0.03	> 0.08	41.827	35.50	> 0.14	0.049	0.04
Total	**117.821**	**100.00**	**Total**	**117.821**	**100.00**	**Total**	**117.821**	**100.00**

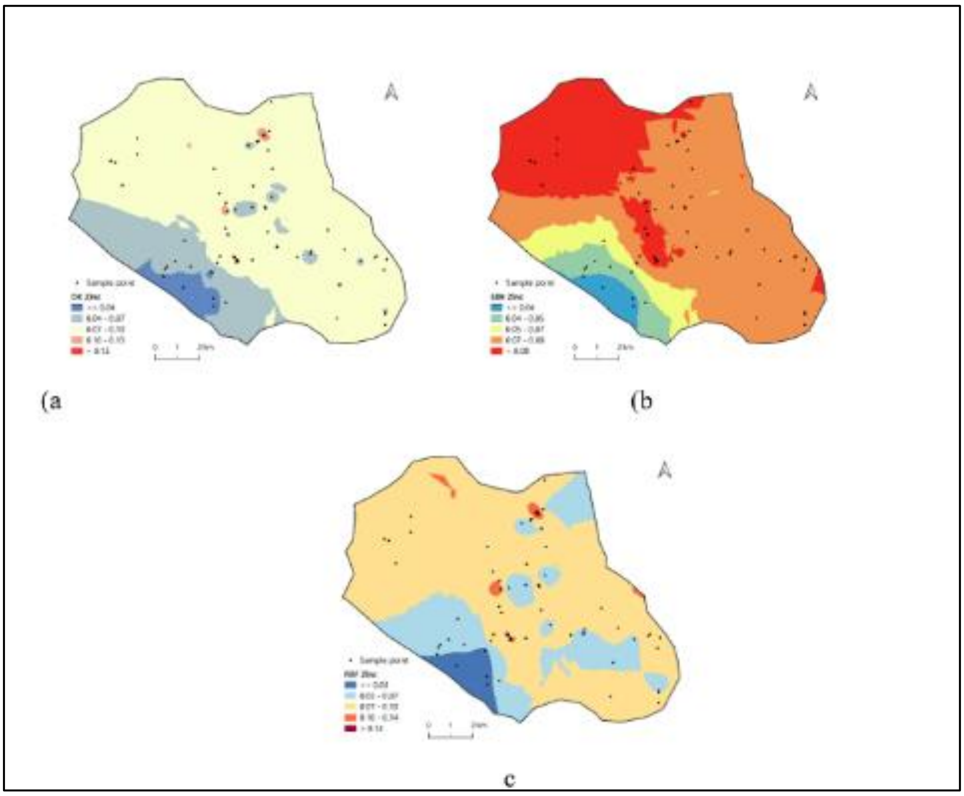

Figure 15 Spatial distribution of Zinc across Asaba. (a) OK, (b). EBK (c) RBF

The only difference is in the shape and the size of the area of different categories. Findings from Fig 15(a) OK reveals that the dominant concentration of zinc (0.07 -0.10) cream colour coded is found in north, south and central of the study area. Fig 15(b) EKB reveals the ranges (0.07 – 0.08) light brown colour coded as the dominant class located in central, east and south while Fig 15(c) RBF reveals the ranges (0.07-0.01) cream colour coded as the dominant class located in entire study area.

4. Conclusion

The present study was designed to elaborate on the use of interpolation methods such as EBK, OK and RBF in predicting the water quality parameters in Asaba, coastal region. The concentration of water quality parameters physiochemical and some heavy metal are Total Suspended Solids, Temperature, Acidity as $CaCO_3$, Alkalinity as $CaCO_3$, Magnesium (Mg), Lead (Pb), Nickel (Ni), and Zinc (Zn) were found below the WHO permissible limits. It was assessed that lead and Zinc values were increasing in the northwest and east of the study area showing similar trend pattern among the three interpolation method use. Result shows that for lead OK gave >0.33 mg/L covers an area of 0.173km^2 (0.15%), for EBK, >0.00052 covers an area of 12.743km^2 (10.83%) while RBF >0.00083 covers an area of 14.122km^2 (11.99%). Zinc contaminants reveals for OK >013 covers an area of 0.034km^2 (0.03%), EBK >0.08 covers an area of 41.827km^2 (35.3%) and RBF >0.14 covers an area of 0.049km^2 (0.04%). This Finding bear similarities with Agyemang 2022 who have lower values in Ghana. The increasing level of Mg in groundwater may cause when in excess laxative effect, cancer and taste issue although it is vital for muscle function and cardiovascular health. This bear similarities with the finding of Ozoko & Iheme 2024 that conduct a study in southern Anambra basin including Asaba. This pollutant is increasing in the northwest and east same pattern of shape from Fig.12 when looking at the three used methods. Cross-validation measures and semi variogram using OK gives better prediction of all the considered parameters and map produced showed the lower quality of this parameters in different parts of the study area. Based on this study we can arrived at saying geostatistical and deterministic techniques are effective in producing high quality spatial distribution maps of groundwater quality parameters. They also serve as reliable tool for predicting locations of unkown sample points using data from measured or collected samples.

Compliance with ethical standards

Acknowledgments

We are thankful to those that have help in different stages of this work.

Disclosure of conflict of interest

The authors declare no competing interest

References

[1] Adeaga, O. A., Aderinto, I. A., & Akinbaloye, O. C. (2019). Effect of Urbanisation on Land Surface Temperature Phenomena in Lags Metropolis. Lagos Journal of Geo-Information Sciences, 6, 47–62.

[2] Agyemang, V. O. (2022): Application of geostatistical techniques in the assessment of groundwater contamination in the Afgya Kwabre District of Ghana; Applied Water Science (2022) 12:53 https://doi.org/10.1007/s13201-022-01582-x

[3] Ayalew, A. A., and Tegenu, M. T. (2024): Spatial Distribution and Trend Analysis of Groundwater Contaminants Using the ArcGIS Geostatistical Analysis (Kriging) Algorithm; The case of Gurage Zone, Ethiopia, DOI: https://doi.org/10.21203/rs.3.rs-5320542/v1

[4] Bhunia, G.S.; Shit, P.K.; Maiti, R.(2018): Comparison of GIS-Based Interpolation Methods for Spatial Distribution of Soil Organic Carbon (SOC). J. Saudi Soc. Agric. Sci. 2018, 17, 114–126.

[5] Bohling, G. (2005) Introduction to geostatistics and variogram analysis. Kansas Geological Survey, Lawrence, pp 1–20

[6] Cambardella, C.A., Moorman, T.B., Novak, J.M., Parkin, T.B., Karlen, D.L., Turco, R.F., & Konopka, A.E. (1994). Field-scale variability of soil properties in central Iowa soils. Soil Science Society of America Journal, 58(5), 1501-1511.

[7] Chaudhry, A. K., Kumar, K., and Afaq Alam, M.(2019): Groundwater contamination characterization using multivariate statistical analysis and geostatistical method . doi: 10.2166/ws.2019.111

[8] Edet, A.E., Okereke, C.S., teme, S. C., & Esu, E.O (2011): Application of remote sensing data to groundwater exploration: A case study of the Cross River State, southeastern Nigeria. Hydrogeology Journal, 19(4), 767-781

[9] ESRI, (2010). ArcGIS Geostatistical Tools for data Exploration, Modeling and Advanced Surface Generation. ESRI White Papers, pp.19

[10] ESRI,(2019). Deterministic Methods for Spatial Interpolation. https://desktop.arcgis.com/fr/arcmap/latest/extensions/geostatistical analyst/deterministic-methodsfor-spatial-interpolation.htm. (Accessed 20 March 2020).

[11] ESRI (2024). ArcGIS Pro 3.x: Geostatistical Analyst Extension Documentation. Environmental Systems Research Institute, Redlands, California

[12] Fallah, B., Richter, A., Wai Ng, K. T., & Salam, A (2019): Effects of groundwater metal contaminant spatial distribution on overlaying kriged maps. Environmental Science and Pollution Research https://doi.org/10.1007/s11356-019-05541-z

[13] Federal Ministry of Water Water Resources (2016): National Water Resource Policy.

[14] Gunnink, J.L.; Burrough, P.A. Interactive Spatial Analysis of Soil Attribute Patterns Using Exploratory Data Analysis (EDA) and GIS. In Spatial Analytical Perspectives on GIS; Routledge: Oxford, UK, 2019; pp. 87–100

[15]

[16] Ibrahim, U.A., Alkali, A.N., Sayaolu, B.O., & Usman, B. (2022): Nigerian water resources management –An overview. Arid zone Journal of engineering, technology and environment, 18(1), 23-30.

[17] Long, D., Chen, X., Scanlon, B.R., Hong, Y.., and Chen, Y. (2016) Have Grace satellites overestimated groundwater depletion in the Northwest India Aquifer?, Sci. Rep., 6 (2016) 243–258

[18] National Environmental standards and regulations enforcement agency (NESREA, 2007)

[19] Nwankwoala, H. O., & Udom, G.J (2015): Influence of urbanization on groundwater quality in Port Harcourt Nigeria. Journal of applied geology and Geophysics, 3(2), 77-86

[20] Oliver, M.A., Webster, R., (1991). How geostatistics can help you. Soil Use Manag. 7, 206–217.

[21] Ozoko, D. C & Iheme, k.O (2024): Evaluation of groundwater resources in part of southern Anambra Basin: its Implications for irrigation Purpose. Journal of environment and earth Science. Vol 14. No 4.

[22] Samsonova, V.P., Blagoveshchenskii, Y.N., Meshalkina, Y.L., 2017. Use of empirical bayesian kriging for revealing heterogeneities in the distribution of organic carbon on agricultural lands. SOIL Chem 50, 305–311. https://doi.org/10.1134/S1064229317030103

[23] Shapiro, S.S. and Wilk, M.B.(1965): An analysis of variance test for normality (complete samples), Biometrika, 52 (1965) 591–611.

[24] Singh, S.K., Singh, P., and Gautam, S.K., (2016). Appraisal of urban lake water quality through numerical index, multivariate statistics and earth observation data sets. Int. J. Environ. Sci. Technol. 13, 445–456.

[25] United Nations Nigeria Annual Report October 2025

[26] World Health Organization (2017). Guidelines for Drinking-Water Quality: Fourth Edition Incorporating the First Addendum. WHO Press, Geneva.

[27] Xie, Y.; Chen, T.; Lei, M.; Yang, J.; Guo, Q.; Song, B.; and Zhou, X.(2011): Spatial Distribution of Soil Heavy Metal Pollution Estimated by Different Interpolation Methods: Accuracy and Uncertainty Analysis. Chemosphere 2011, 82, 468–476.